Exploration of Carbon Allotropes with Four-membered Ring Structures on Quantum Chemical Potential Energy Surfaces

Koichi Ohno, *[a,b] Hiroko Satoh,[a,c,d] Takeaki Iwamoto,[b] Hiroaki Tokoyama,[a] and Hideo Yamakado[e]

The existence of a new carbon allotrope family with four-membered rings as a key unit has been recently predicted with quantum chemical calculations. This family includes carbon allotropes in *prism-*, *polymerized prism-*, *sheet-*, *tube-*, and *wavy-*forms. An atypical bond property has been observed in this series of carbon structures, which differs from the typical sp^3, sp^2, and sp hybridizations. The lowest energy barrier from some of the equilibrium states of the carbon structures has been determined with the SHS-ADDF (scaled-hypersphere-search combined with the anharmonic downward distortion following) method within the GRRM software program package. The height of the barriers indicates that the well is deep enough for the carbon structures to exist. This class of carbon allotropes is expected to be energy-reservoirs with extra energy of 100–350 kJ mol^{-1} per one carbon atom. This article presents the structures, energies and reactivity of the carbon allotropes with four-membered ring structures as well as the background of the findings in the context of the global exploration of potential energy surfaces. © 2018 Wiley Periodicals, Inc.

DOI:10.1002/jcc.25556

Introduction

Carbon is a ubiquitous element that composes many kinds of substance.[1] Various kinds of carbon allotropes are known, such as diamond, graphite, fullerenes,[2] carbon nanotubes,[3] and graphenes.[4] Carbon atoms can form covalent bonds from single to triple bonds and also the noncovalent types of bond formed due to a weak force, for example, the van der Waals bond. The typical CC bond-lengths of the triple, double, conjugated double, single, and van der Waals bonds are about 0.12, 0.13, 0.14, 0.15, and 0.34 nm, respectively. The CCC bond angle can take a wide range from 60° to 180°, which can be found for various types of hydrocarbons, such as cycloprpane (60°), cubane (90°), benzene (120°), and allene (180°). The valence theory of chemical bonds[5] can be applied to understand the structures and properties of a wide range of chemical structures, and various important carbon structures have been discovered within the valence bond theory. For instance, there is a carbon nanobelt family,[6] which has been recently developed within the valence bond theory. They are composed of hexagonal benzenoid rings, which are familiar aromatic hydrocarbons such as phenanthrene and chrysene. The carbon element still shows us unexpected structures, which can be not only within the valence bond theory but also beyond this theory.

The recent developments of computational chemistry have provided advanced methods to search the stationary points and reaction pathways on potential energy surfaces (PES), which can be applied to the elucidation of chemical structures and reactions.[7,8][7,8] Chemical structures can be found as minima or equilibrium points (EQs), and transition structures (TSs) are located at the first-order saddle points on PES. The reaction pathways from a TS can be calculated as the intrinsic reaction coordinates (IRCs),[9] which lead to EQs or dissociation channels (DCs) to the forward and the backward directions from the saddle point. TSs are often difficult to be located on PES in the reaction analysis. A solution of this problem was given by the methods called the anharmonic downward distortion following (ADDF) in 2004[10–12] and the artificial force induced reaction (AFIR) methods in 2010.[13–15] Both of the methods can be applied to the systematic exploration of global reaction route mappings (GRRM).[16]

The purpose of this article is to review the computational studies on the exploration of new carbon structures based on quantum chemical calculations of PES. Carbon structures have been intensively studied, and a comprehensive review about various forms of carbon structures was published in 2015.[17] Theoretical studies concerning low-lying crystal structures have been also recently reviewed.[18] Therefore, we will focus only on our recent findings of a new class of carbon structures, which

[a] *K. Ohno, H. Satoh, H. Tokoyama*
Institute for Quantum Chemical Exploration, Kaigan 3-9-15, Minato-ku, Tokyo 108–0022, Japan
E-mail: ohnok@m.tohoku.ac.jp
[b] *K. Ohno, T. Iwamoto*
Department of Chemistry, Graduate School of Science, Tohoku University, Aramaki Aza-Aoba 6-3, Aoba-ku, Sendai, Miyagi, 980–8578, Japan
[c] *H. Satoh*
Department of Chemistry, University of Zurich, 8057, Zurich, Switzerland
[d] *H. Satoh*
Research Organization of Information and Systems (ROIS), Tokyo 105-0001, Japan
[e] *H. Yamakado*
Faculty of Systems Engineering, Wakayama University, Sakaedani 930, Wakayama, 640-8510, Wakayama, Japan
Contract Grant sponsor: Japan Society for the Promotion of Science;
Contract Grant number: 23655021, 25540017

include four-membered rings as a key unit.[19–22] These carbon structures consist of an atypical bond property, which does not belong to any of the typical sp^3, sp^2, and sp hybridizations. We have theoretically indicated the possibility of the existence of this class of carbon structures in prism-,[19] polymerized prism-,[20] sheet-,[20] tube-,[21] and wavy forms.[22] We will describe the details of the geometries and electronic structures of them as well as the background of the studies related to the known structures of hydrocarbons with four-membered carbon rings, for example, cyclobutadiene and prismanes. The idea of this carbon structure project was risen through the stimulus discussions at the symposium for celebrating 80th anniversary of Professor Dr. Keiji Morokuma, which was held on January 23, 2015, at Fukui Institute for Fundamental Chemistry in Kyoto, Japan.

Computational Methods

The Gaussian 09 program (G09)[23] was used for the electronic-state calculations. The GRRM14[24] software program package was used for (1) a geometry optimization starting from a given initial structure, (2) finding energy barriers from an EQ, and (3) a global PES exploration for a given atomic composition specified with a molecular formula. Detailed specifications of the calculations will be shown in the following sections.

Exploration of structures and reaction pathways with SHS-ADDF

The explorations of structures and reaction pathways in this study were done by using the scaled-hypersphere-search (SHS) method combined with the ADDF technique (SHS-ADDF)[10–12] within GRRM14. SHS-ADDF is used to trace on PES. It makes it possible to find all of the reaction pathways and TSs from an EQ. This method uses scaled hyperspheres at the energy minima to detect the uphill directions of reaction pathways toward TS. Once a TS is found, IRCs are confirmed, which trace from the TS to both of the downhill directions to reach EQ or DC, by a conventional technique, such as the steepest decent method.[7,8] This procedure is repeated at all of the located EQs and produces a reaction channel network, which is composed of EQ-TS-EQ and EQ-TS-DC pathways.[10–12]

Confirmation of chemical bonds using QTAIM

The property of Chemical bonds was confirmed as the bond paths in a molecular graph defined in the scheme of the Quantum Theory of Atoms in Molecules (QTAIM),[25] which is implemented in AIM2000[26] software. We calculated the bond paths values based on the electron-density distributions obtained by using G09.

Periodic boundary condition calculations

Optimization of the periodic structures was performed in the periodic boundary conditions (PBC) by using G09. The periodic structures were calculated at the RHF/STO-3G level. The initial translational vectors were specified in each of the cases so as to form appropriate CC bonds between adjacent units.

Results and Discussions

Global exploration of isomers and reaction pathways for C_4H_4

We started with a global PES exploration in the ground singlet state for C_4H_4 by SHS-ADDF method to find all the isomers with reaction pathways and obtained 32 EQs and 171 TSs at the B3LYP/6–31G(d) level.[19] We chose this level to reduce computational cost. The decision was made also based on the fact that the calculations for H_2CO at the restricted B3LYP/6–31G(d) level explored the same major structures in low energy as those explored at the unrestricted level, which gave in addition some configurations in considerably high energy such as radical fragments and roaming channels.[27,28]

Part of the explored results by the B3LYP/6–31G(d) level is shown in Figure 1. The EQs are the minima, which are with the serial numbers in ascending order of the potential energy. The relative energy with respect to EQ0 is shown for each EQ. The number labeled on a line connecting two EQs is the TS energy relative to EQ0. The energy unit is kJ mol^{-1}. The EQ0 is the most stable isomer, vinylacetylene HC≡C—CH═CH_2 (**1**). The second lowest isomer EQ1 is cumulene **2**, H_2C═C═C═CH_2 (D_{2h}, 8.0 kJ mol^{-1}). The third EQ2 is methylenecyclopropane **3** (C_{2v}, 85.3 kJ mol^{-1}).

The results showed that cyclobutadiene **4** (EQ4) is a relatively stable isomer: This is located at the third hop of the reaction path from **1** to tetrahedrane **5** (EQ15), where the highest energy barrier is 412.3 kJ mol^{-1} between EQ9 and **4** (EQ4). The four-membered ring is a known structure unit, which composes cubane, for example, but has gotten less attentions compared to the larger rings, such as five-, six-, and seven-membered rings. However, the results inferred the possibility of the existence of more structures with four-membered rings.

Partial exploration of isomers and reaction pathways for C_6H_4

A next target for the exploration of isomers and reaction pathways was C_6H_4. We conducted exploration calculations limited to low energy isomers instead of global search, so that we would be able to determine the energy level of the structures with four-membered rings relative to the isomers in rather low energy level.[19] We did the calculations by the large-ADDF (LADD) option of the GRRM14 program and obtained 356 EQs and 1061 TSs with LADD = 5 at the B3LYP/6–31G(d) level.

The global, second, third, and fourth minima within this search were *o*-benzyne **6** (1,2-didehydrobenzene, EQ0, C_{2v}), *m*-benzyne **7** (bicyclo[3.1.0]hexa-1,3,5-triene, EQ1, C_{2v}, 46.7 kJ mol^{-1}), vinyl diacetylene **8** (hex-1-en-3,5-diyne, EQ2, C_1, 48.0 kJ mol^{-1}), and 1,2,3,4,5-hexapentaene **9** (EQ3, D_{2h}, 70.4 kJ mol^{-1}), respectively. The highest minimum was EQ355 with 684.0 kJ mol^{-1} relative to the global minimum EQ0. Some of the interesting isomers of C_6H_4 explored in this study are shown in Figure 2. There are several structures with four-membered rings, including butalene (**10**), EQ22. The structure **10** was in a D_{2h} symmetry with 240.3 kJ mol^{-1} relative to EQ0. This is the 23rd minimum and is accounted to be a rather low energy level.

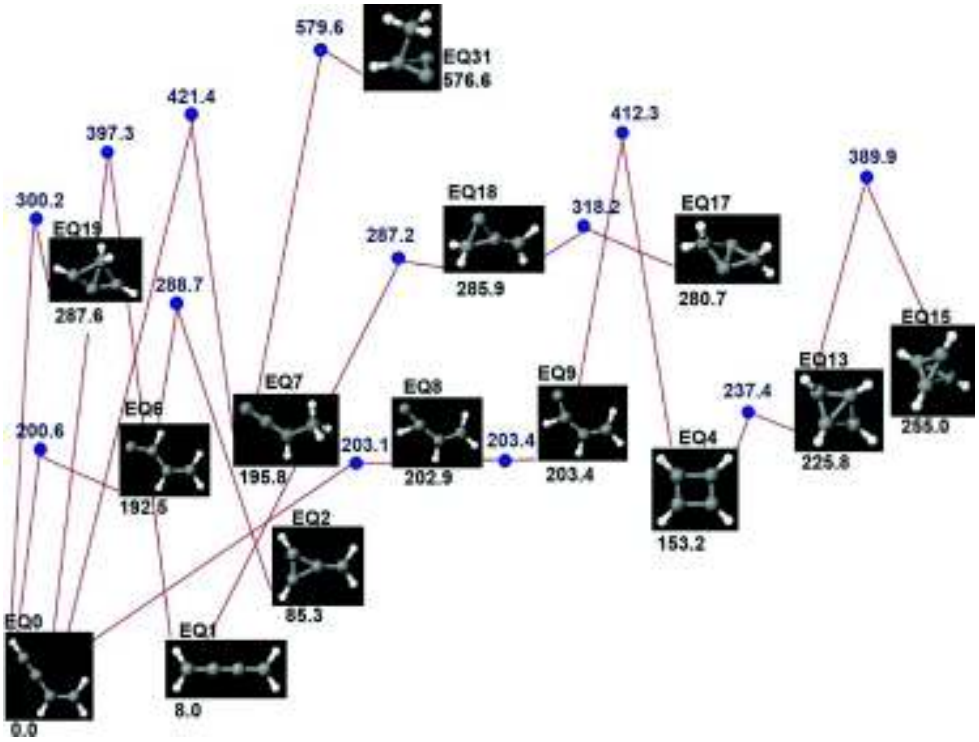

Figure 1. Part of the reaction channels for C_4H_4. TSs are shown as blue dots with their energies in kJ mol^{-1}.

Exploration of ladder carbons

The stability of butalene **10** observed in the C_6H_4 isomer exploration encouraged us to increase the number of four-membered rings toward a ladder form. Then, we extended it to $C_{10}H_4$ (**11**) and obtained a structure in a C_{2v} symmetry at the B3LYP/6–31G(d) level.[19] The optimized structure formed a curve shape, whereas C_4H_4 and C_6H_4 are in a planar shape of a D_{2h} symmetry (Fig. 3). The central CCC bond angle along the ladder edge was 142°. We increased the number of carbon atoms and conducted geometry optimizations of $C_{2n}H_4$ starting from a planer shape and found that they converged to a wavy form in different patterns, which led us to find wavy carbons, as will be seen in a later section.

Exploration of prism-C_{2n}

The curved ladder structures gave us a hint to build a circular ladder structure without hydrogen atoms, and we obtained a C_{20}, which is composed of two decagon rings connected to each other with 10 vertical bonds, in a D_{10h} symmetry at the B3LYP/6–31G(d) level (Fig. 4).[19] We named this new carbon allotrope prism-C_{20} **12**. The length of the bond in the decagon ring is 0.144 nm, and that of the vertical bond is 0.148 nm. These lengths lay between single (ca. 0.154 nm) and aromatic (ca. 0.140 nm) CC bonds. The bond angle of each of the squares is 90.0°. All of the Hessian eigenvalues were found to be positive that confirmed the local minimum structure. We performed further geometry optimizations in the ground singlet state at

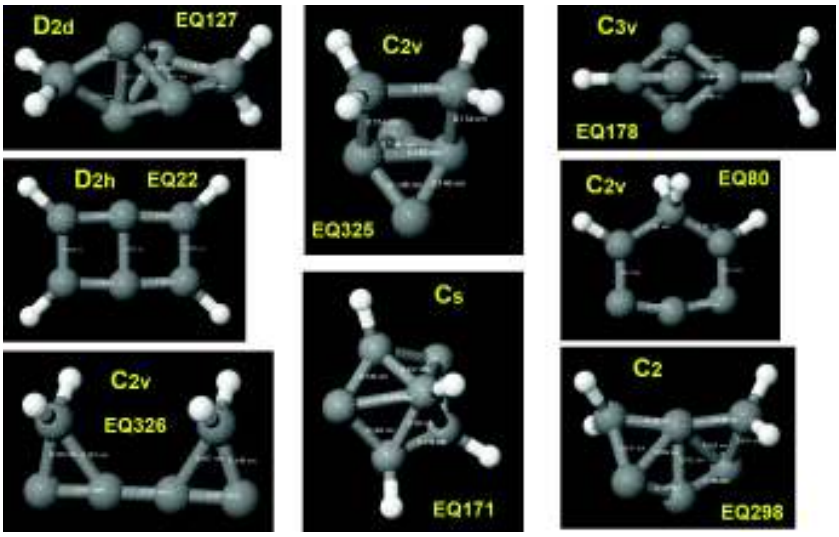

Figure 2. Some interesting isomers of C_6H_4 found by the exploration limited to low energy structures. The EQs are numbered in the ascending order of energy relative to *o*-benzyne (**6**), the global minimum EQ0 within this search.

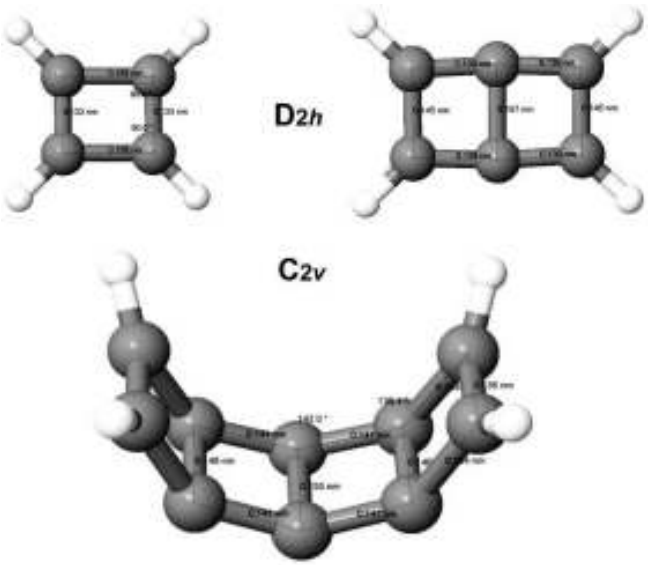

Figure 3. Ladder carbon structures. Cyclobutadiene C_4H_4 **5** (top left, D_{2h}), butalene C_6H_4 **10** (top right, D_{2h}), and a condensed cyclobutadienoid $C_{10}H_4$ **11** (bottom, C_{2v}).

the B3LYP/6–311++G(d,p), B3LYP/6–311++G(2d,2p), B3LYP/cc-pVDZ, and B3LYP/cc-pVTZ levels to make sure the optimized structure and obtained the same geometry in three digits of the xyz-coordinates as that obtained at the B3LYP/6–31G (d) level. The relative energy of **12** per one carbon atom was determined to be 135.14 kJ mol^{-1} with respect to the fullerene C_{60} molecule at the B3LYP/6–31G(d) level.

We confirmed the chemical bond property of **12** based on the bond paths values (Fig. 5). Figure 5A shows that the carbon atoms are connected by the bond paths with bond-critical points (BCP) denoted as red dots. The electron densities at the BCPs are 0.2700 and 0.2688 au for the ring and the side bonds, respectively. They are in the normal values indicating ordinary chemical bonds, whereas the other regions show lower density: The electron density at the ring critical points (RCP, yellow dots) at the center of squares and at the center of the decagon rings are 0.1090 and 0.0012 au, respectively, and that of the cage critical point (CCP, a green dots) at the body center is 0.00077 au.

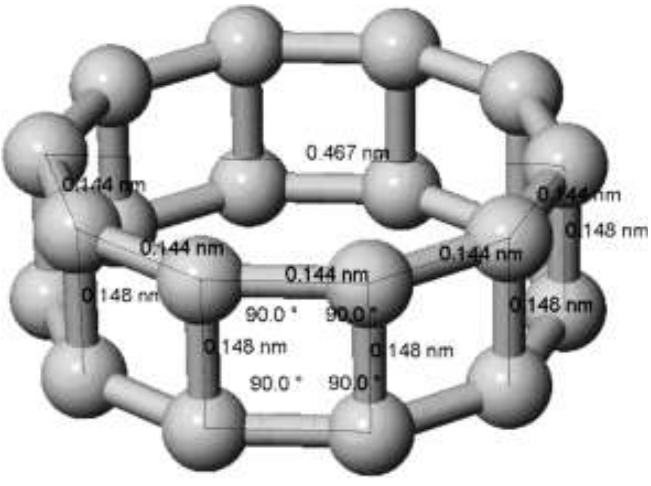

Figure 4. Prism-C_{20} **12** in D_{10h}

The van der Waals surface is shown in Figure 5B. The size of **12** can be estimated from its diameter of 0.465 nm and the side bond length of 0.148 nm as well as the van der Waals radii of carbon, 0.170 nm. The thickness of the van der Waals envelope of **12** is 0.488 nm, the outer diameter is 0.807 nm, and the inner diameter of the hole is 0.127 nm. The size of the inner hole seems to be too small for repulsive particles, but it may capture some positive ions with attractive forces.

Figures 5C–5E show electron density contours for the ring plane, the square plane, and the cutting plane, respectively. The outer thick curves at the density of 0.004686 au indicate the molecular surface corresponding to the van der Waals surface. The contour curves are shown at $\rho = a \times 2n$, where $a = 0.00625$ au and $n = 0, 1, 2, \cdots$. The BCP, RCP, and CCP points are also shown in Figures 5C–5E. The doughnut hole of the molecular surface can be recognized in Figures 5B, 5C, and 5E.

We investigated the reaction channels associated to **12** in a D_{10h} symmetry by using the SHS-ADDF method.[10–12] The lowest barrier of the reaction pathway from **12** was 158.0 kJ mol^{-1} (1.638 eV) after the zero point vibrational energy (ZPVE) corrections. This barrier is much larger than thermal energies. This is a reaction of bond breaking at the two neighboring side bonds (**13**, Fig. 6). The octagon ring in **13** is fused with the two decagon rings by sharing double, triple, and double bonds. This alternate double and triple bond pattern is the same as that in the monocyclic C_{20} ring.[19] It is assumed that the side bond is more breakable than the bond in the decagon ring because of the higher stability of the decagon rings. This new carbon allotrope **12** with a large relative energy per one carbon atom (135.14 kJ mol^{-1}) but with the thermal stability may possibly have a function to be a chemical energy reservoir.

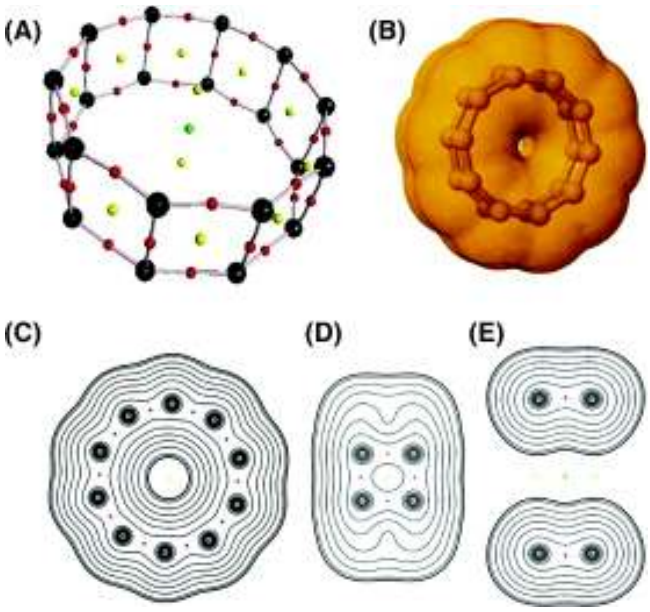

Figure 5. A) Bond paths and electron-density critical points of prism-C_{20} **12**. B) The van der Waals surface. C) Electron density contours for the ring plane. D) Electron density contours for the square shape including neighboring side bonds. E) Electron density contours for the cutting plane including the central symmetry axis and four carbon atoms.

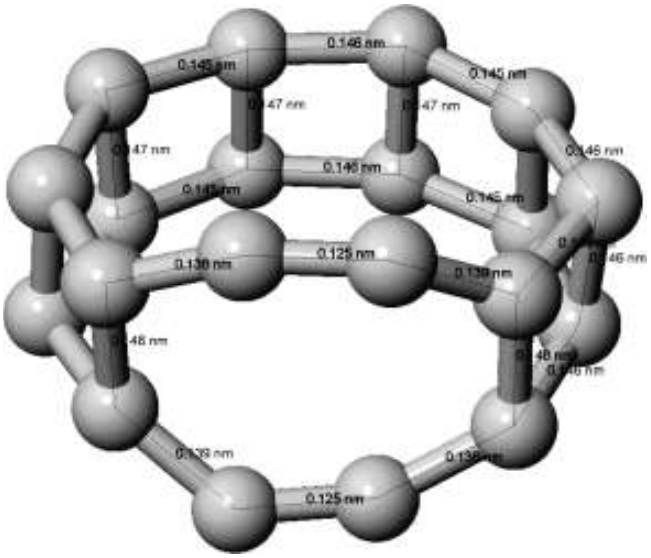

Figure 6. Reaction product **13** via a lowest barrier from prism-C_{20} **12**.

We investigated several sizes of the prism C_{2n} (n = 6, 7, 8, 9, 10, 12, 14, 16, 18, 20) at the B3LYP/6–31G(d) level and determined the structures for all of the sizes in C_{3v}, C_s, D_{8h}, D_{3h}, D_{10h}, D_{4h}, D_{14h}, C_{8v}, C_{2h}, and D_{20h} symmetry, respectively. The structures excepting n = 6 and 7 are shown in Figure 7. The polygons of C_{16} (n = 8), C_{20} (n = 10), C_{28} (n = 14), and C_{40} (n = 20) were a regular form with the same bond lengths in the ring, whereas the polygons of C_{12} (n = 6), C_{14} (n = 7), C_{18} (n = 9), C_{24} (n = 12), C_{32} (n = 16), and C_{36} (n = 18) were slightly deformed from the regular polygons. The energies and bond lengths of prism-C_{2n} are listed in Table 1. The prism-C_{2n} larger than n = 20 could not be determined. Instead, we found that the large polygons turned to be in a wavy form. This finding led us to determine another type of carbon allotropes called wavy carbons, as will be described in a later section.

Exploration of polymerized prism-C_{2n}.

The findings of the prism-C_{2n} structures stimulated us to explore the diversity of the carbon structures with four-membered rings as a key unit. Then, we investigated the possibility of several types of carbon allotrope and determined polymerized prism-C_{2n},[20] prism-C_{2n} sheets,[20] prism-C_n tubes,[21] and wavy C_n structures.[22] We will describe about the polymerization of prism-C_{2n} in this section.

The bond lengths of prism-C_{2n} are in about 0.144–0.148 nm. They are shorter than the typical single bond (0.154 nm) and are assumed to have unsaturated bond characters. Therefore, we decided to explore the possibility of the polymerization of prism-C_{2n} and obtained a dimer of prism-C_{16} (**14**, Fig. 8A) and a trimer of prism-C_{24} (**15**, Fig. 8C) structures.

Geometry optimization calculations were done with adequate cares for tightness of minimization, updating timing of Hessians, and ultra-fine grids in density functional calculations. Harmonic vibrational modes were calculated to confirm stable equilibrium structures with no imaginary frequencies as well as to perform ZPVE corrections. Initial minimization calculations for **14** and **15** were done at the B3LYP/6–31G(d) level starting from two prism-C_{16} units in a D_{8h} symmetry and from three prism-C_{24} units in a D_{12h} symmetry, respectively. They were placed in parallel to face one another at their four-membered rings with a distance of 0.157 nm. The initial structure of the trimer was a set of the three units arranged to be trigonal and joined each other via cuboid bridges at a threefold symmetry. We optimized the results at the B3LYP/6–31G(d). Further, re-optimization calculations were performed at the higher levels of B3LYP/6–311++G(2d,2p), B3LYP/cc-pVDZ, and B3LYP/cc-pVTZ and confirmed the obtained geometries to be very similar to that at the B3LYP/6–31G(d) level. The chemical bond properties in those equilibrium structures were well reproduced even at the lower levels, such as RHF/STO-3G and RHF/3-21G.

The dimer of prism-C_{16} **14** converged to a D_{2h} symmetry as shown in Figure 8A. The lengths of the bonds in the cuboid bridge and belonging to the octagon rings (C1—C8, C9—C16, C1′—C8′, and C9′—C16′) are about 0.161 nm, and the other bonds in the cuboid bridge are about 0.158 nm, which are in the range of the CC single bond. This means, that the cuboid bridge is composed of single bonds. The prism structures in **14** are slightly deformed from the D_{8h} symmetry of the original prism-C_{16} structure (0.143 nm on the octagon, and 0.153 nm on the side):[19] The lengths of the vertical bonds, C1—C1′, C2—C2′, C3—C3′, and C4—C4′, are 0.158 nm, 0.147, 0.161, and 0.147 nm, respectively. The lengths of the horizontal bonds in the octagon rings, C1—C8, C1—C2, C2—C3, C3—C4, and C4—C5, are 0.161, 0.151, 0.141, 0.141, and 0.151 nm, respectively. We noticed that the lengths of C2—C3 and C3—C4 were rather short (0.141 nm), which is in the range of unsaturated CC bonds. Then we came up with an idea to look into the possibility of further polymerization of these units and obtained sheet structures composed of the prism-C_{16} units, as will be shown in the next section.

Figure 8B shows the results of the bond paths analysis for **14** in the same manner as that in Figure 5. The electron density values on the BCPs at the four joint bonds are all 0.217 au, and those at the prisms are between 0.202 to 0.291 au. These values indicate that the chemical bonds drawn in Figure 8A are relevant. The electron density values on the RCPs at the center of the squares are between 0.07 and 0.11 au, and those at the center of the octagon rings are all 0.004 au. The electron density value on the CCPs at the body center of the cuboid bridge

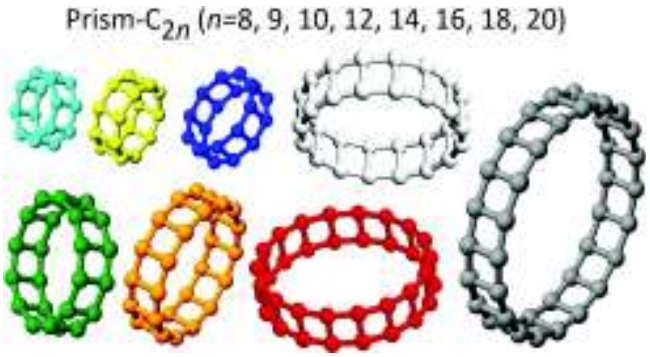

Figure 7. C_{16}, C_{18}, C_{20}, C_{24}, C_{28}, C_{32}, C_{36}, and C_{40} of the prism carbon family confirmed by B3LYP/6–31G(d) calculations.

Table 1. Relative energies per one carbon atom (kJ mol^{-1}) and bond lengths (nm) for prism and wavy carbon structures.[a]

	Relative energy (EI)[b]	Vertical bond length[c]	Bond length in polygon[d] 1–2 2–3 3–4 4–5 5–6
Prism-C_{16} (D_{8h})	133.87	0.153	0.143
Prism-C_{18} (D_{3h})	140.35	0.152 0.148	0.146 0.140
Prism-C_{20} (D_{10h}) **12**	135.14	0.148	0.144
Prism-C_{24} (D_{4h})	141.59	0.146 0.157	0.141 0.157
Prism-C_{28} (D_{14h})	138.36	0.151	0.143
Prism-C_{32} (C_{8v})	141.07	0.148	0.143 0.146
Prism-C_{36} (C_{2h})	143.05	0.146 0.157	0.141 0.151
Prism-C_{40} (D_{20h})	142.38	0.150	0.144
D_{6h} prism-C_{12} sheet A **16**	96.65	0.156	0.157
D_{2h} prism-C_{12} sheet B **17**	129.02	0.158 0.156	0.157 0.158
D_{4h} prism-C_{16} sheet C **18**	136.97	0.157	0.156 0.158
D_{6h} prism-C_{24} sheet D **19**	148.73	0.157	0.156 0.158
D_{4h} prism-C_{24} sheet E **20**	160.34	0.157 0.133	0.153 0.158
Prism-C_3 tube	252.92	0.159	0.153
Prism-C_4 tube	242.16	0.160	0.158
Prism-C_5 tube	217.81	0.160	0.157
Prism-C_6 tube	226.90	0.160	0.157
Prism-C_7 tube	244.26	0.160	0.157
Prism-C_8 tube	257.83	0.160	0.157
Prism-C_{10} tube	285.95	0.161	0.158
Prism-C_{12} tube	307.07	0.161	0.158
Prism-C_{14} tube	323.33	0.161	0.159
Prism-C_{16} tube	336.10	0.161	0.159
Prism-C_{18} tube	346.20	0.161	0.159
Prism-C_{20} tube	354.34	0.161	0.160
Wavy-C_2 sheet **28**	205.92	0.161	0.154
Wavy-C_6 sheet **29**	229.19	0.161	0.154 0.158
Wavy-C_8 sheet **30**	241.80	0.161	0.153 0.158 0.159
Wavy-C_{36} tube **31**	252.89	0.161	0.158 0.153 0.157 0.159 0.160

[a] Calculation levels were B3LYP/6–31G(d) for prsim-C_{2n} and RHF/STO-3G for prism sheets, prism tubes, and wavy carbons.
[b] Relative energies are given per one carbon atom, and denoted as energetic index, EI (see text). For prsim-C_{2n}, relative energies are measured with respect to fullerene C_{60} molecule. For wavy carbons, prism tubes, and prism sheets, relative energies are measured with respect to graphene.
[c] Lengths of the bonds vertical to the largest polygon. For nonequivalent bonds, values are added.
[d] Lengths of the bonds in the polygon. For nonequivalent bonds, values are added, according to the numbering in respective figures.

is 0.028, and the both values at the body centers of the prisms are 0.004 au. These electronic density values are much smaller than that on the BCPs.

The trimer of prism-C_{24} **15** converged to a D_{3h} symmetry as shown in Figure 8C. The lengths of the 12 bonds in the cuboid bridge but not belonging to the decagon rings (e.g., C12—C13 and C11—C14) are 0.157–0.159 nm. The results show that the cuboid bridges are composed of single bonds. This is the same tendency observed in the dimer **14**. The lengths of the bonds in the decagon rings (e.g., C1—C2 and C2—C3) are between 0.135 and 0.159 nm, and the lengths of the vertical bonds at the side faces (e.g., C1—C1′ and C2—C2′) are between 0.144 and 0.162 nm. As we saw in the octagon rings of **14**, we found the unsaturated type of bond lengths (0.135–0.141 nm) also in

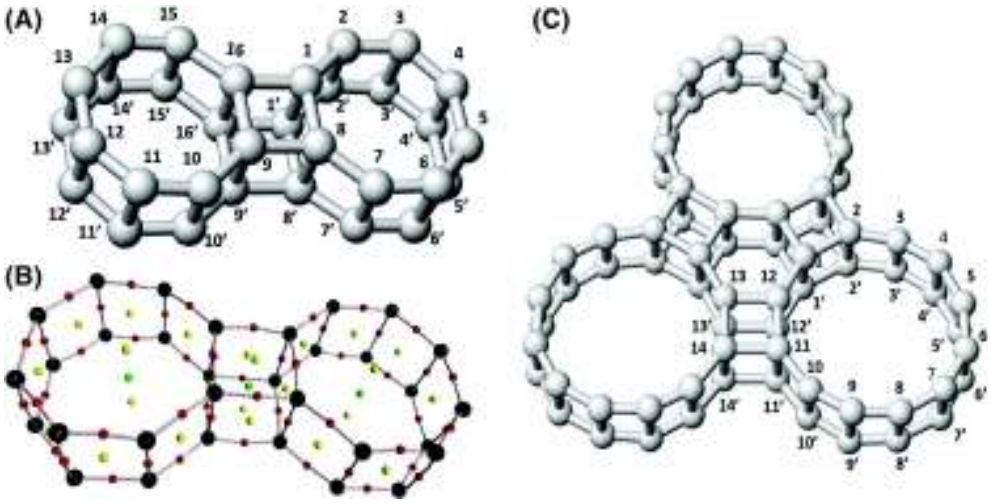

Figure 8. Prism-C_{16} dimer **14** in D_{2h} and Prism-C_{24} trimer **15** in D_{3h}. A) Two prism-C_{16} units of **14** are connected to each other via four joint single bonds in a cuboid bridge. B) Bond paths and electron density critical points of **14**. A bond path with a BCP is shown as a red dot. RCP and CCP are denoted as yellow and green dots, respectively. C) Three prism-C_{24} units of **15** are connected to each other with four joint single bonds in a cuboid bridge.

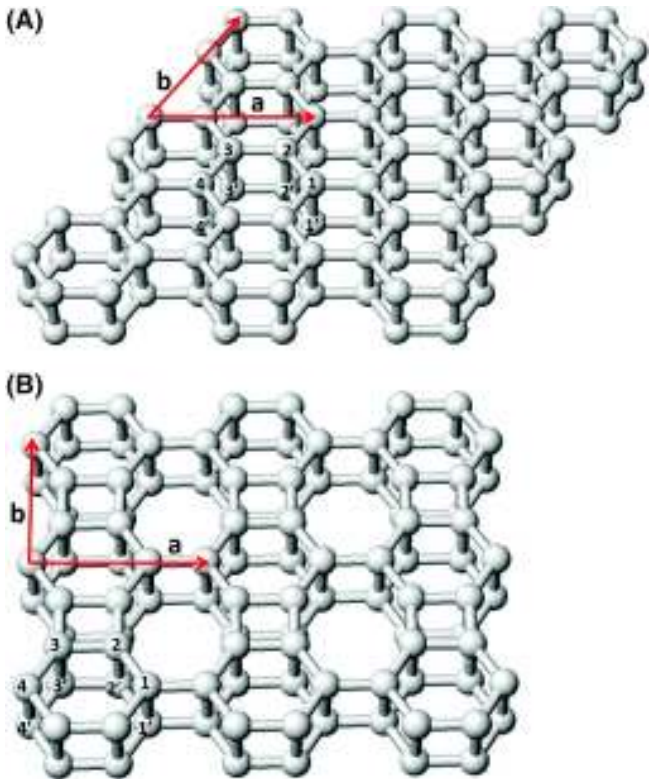

Figure 9. Two types of prism-C_{12} sheets. A) Prism-C_{12}-sheet-A in a D_{6h} symmetry (**16**). Prism-C_{12} units are condensed forming a hexagonal sheet of equivalent carbon atoms bonded with four adjacent carbon atoms. B) Prism-C_{12}-sheet-B in a D_{2h} symmetry (**17**). Prism-C_{12} units are connected by cuboid bridges in the y-direction and by rectangle bridges in the x-direction.

the dodecagon rings at C3—C4, C4—C5, and C6—C7, which led us to the sheet structures.

The height of the lowest energy barriers from **14** was 34.3 and 33.4 kJ mol^{-1} at the B3LYP/6–31G(d) and B3LYP/cc-pVDZ levels, respectively. The barriers are associated to the same reaction, where two vertical bonds belonging to the cuboid bridge and to the same prism structure (e.g., C1—C1′ and C8—C8′) undergo breaking. The energy of the reaction product was −632.5, and − 625.8 kJ mol^{-1} relative to **14**, at the B3LYP/6–31G(d) and B3LYP/cc-pVDZ levels, respectively. The height of the lowest energy barrier from **15** at the B3LYP/6–31G(d) level was 30.3 kJ mol^{-1}, which is associated to a reaction, where two adjacent vertical bonds belonging to the same cuboid bridge and to different prism structures (e.g., C11—C11′ and C14—C14′) undergo breaking. The energy of the reaction product was −583.4 kJ mol^{-1} relative to **15** at the B3LYP/6–31G(d) level. The energy barrier of about 30 kJ mol^{-1} (ca. 2500 cm^{-1}) corresponds to the range of the binding energies of hydrogen bonds (1–-155 kJ mol^{-1}). The results indicate that these polymerized prism-C_{2n} structures would be stable enough to observe at low temperature but are thermally metastable at high temperature.

Exploration of prism-C_{2n}-sheets

Next direction of the exploration was to double–layered carbon sheet structures. The prism-C_{2n}-sheet structures were constructed by arranging the prism-C_{2n} units (n = 6, 8, and 12) in several patterns.[20] It is a kind of extension of the polymerized prism-C_{2n}. The calculations were done at the RHF/STO-3G level. Prism–C_{12} and C_{16} sheets were calculated also at the RHF/3-21G level. The unit cell of PBC contains one prism structure, which was initiated from a regular polygon prism with the bond lengths in the polygons and the vertical side bonds to be 0.144 and 0.150 nm, respectively. Initial two-dimensional (2D) translation vectors were set to be at an angle of 60° or 90° with a nearest distance of 0.157 nm between the prism-C_{2n} units. All of the coordinates were optimized in the repeated procedures of the PBC calculations. The energies relative to the graphene sheet were estimated at the same calculation level and were normalized per one carbon atom to compare between different sizes of carbon unit-cell.

The geometry optimization calculations with the 2D PBCs resulted in the several types of periodic arrays of prism carbons as shown in Figures 9–11: prism-C_{12}-sheet-A in a D_{6h} symmetry (**16**, Fig. 9A), prism-C_{12}-sheet-B in a D_{2h} symmetry (**17**, Fig. 9B), prism-C_{16}-sheet-C in a D_{4h} symmetry (**18**, Fig. 10), prism-C_{24}-sheet-D in a D_{6h} symmetry (**19**, Fig. 11B), and prism-C_{24}-sheet-E in a D_{4h} symmetry (**20**, Fig. 11B). The calculations were done for infinite systems, but the lattices cut at certain ranges are visualized in Figures 9–11. Translation vectors **a** and **b** are shown by arrows. As will be described below, all of the bonds in **16**–**19** are considered to be single bonds according to the bond lengths. Both of the single- and double-bond lengths are observed only in **20**.

The type of all the carbon atoms of **16** is equivalent: Each of the carbon atoms connects to four atoms. The bond lengths of the hexagonal bonds and vertical bonds are 0.1566 and 0.1562 nm at the RHF/STO-3G level, and 0.1566 and 0.1583 nm at the RHF/3-21G level, respectively. The structure of **16** looks like a double layered graphene sheets, but all of the bonds are single bond. This suggests that the prism **16** has a different property of an electron system from the π electron conjugation system.

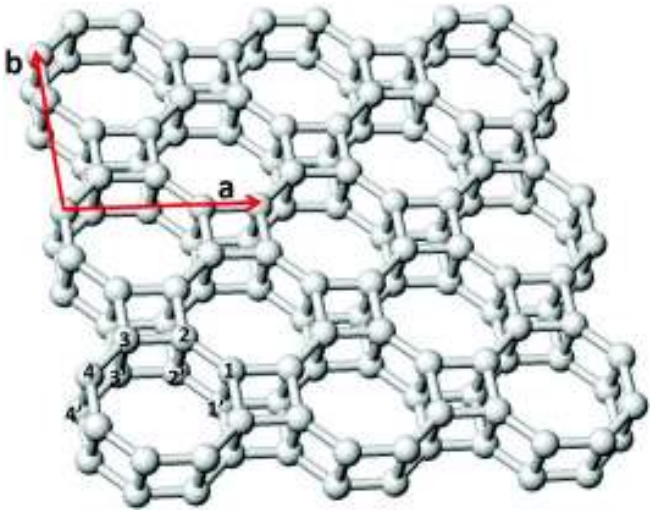

Figure 10. Prism-C_{16}-sheet-C in a D_{4h} symmetry (**18**). Prism-C_{16} units are connected by cuboid bridges in both of the x- and y-directions.

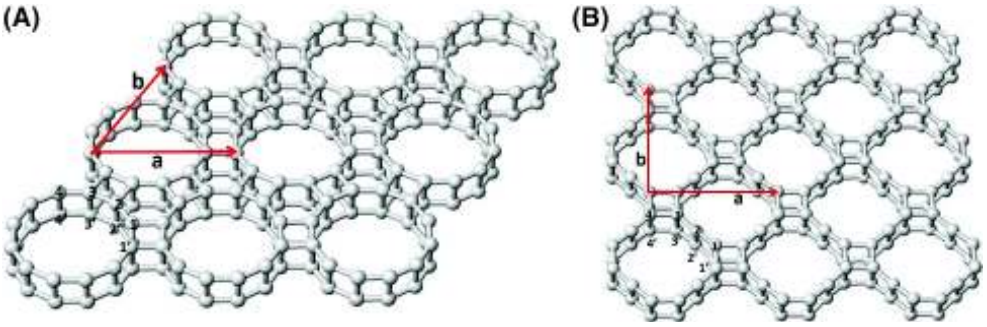

Figure 11. Two types of the prism-C_{24} sheet. A) Prism-C_{24}-sheet-D in a D_{6h} symmetry (**19**). B) Prism-C_{24}-sheet-E in a D_{4h} symmetry (**20**). Prism-C_{24} units are connected by cuboid bridges in both of **19** and **20**.

Different bond lengths were observed in the cuboid and rectangular bridges of **17**. The bond lengths of the vertical bonds in the cuboid and rectangular bridges are 0.1561 and 0.1580 nm at the RHF/STO-3G level, and 0.1579 and 0.1607 nm at the RHF/3-21G level, respectively. Therefore, the shape of the sheet is not completely flat. The horizontal bond lengths are in the range between 0.156 and 0.160 nm. All of the vertical bond length of **18** are the same, which is 0.1568 and 0.1590 nm at the RHF/STO-3G and RHF/3-21G levels, respectively, that means, it is completely flat. The horizontal bond lengths in the bridges are longer than the others: The horizontal and the other bond lengths are 0.1577 and 0.1558 nm at the RHF/STO-3G level, and 0.1591 and 0.1553 nm at the RHF/3-21G level, respectively. The cuboid bridges in **18** are approximately cubic with almost the same bond length of 0.1568–0.1577 and 0.1590–0.1591 nm at the RHF/STO-3G and RHF/3-21G levels, respectively.

The structure **19** is composed of dodecagon prisms connected to each other by the joint bonds of 0.1578 nm in the cuboid bridges. All of the vertical bond length of **19** are the same, which is 0.1567 nm, that means, it is completely flat. The bond lengths of the dodecagon rings are 0.1561–0.1579 nm, which are slightly deformed from the regular dodecagon in a D_{12h} symmetry.

The decagon prism structures in **20** are considerably deformed from the regular dodecagon prism. The vertical bond length in the cuboid bridges (e.g., C1—C1′) is 0.1574 nm, and the other vertical bond length (e.g., C2—C2′) is 0.1327 nm. This double bond property is observed only for the vertical bonds of the cuboid bridges. The horizontal bond lengths (e.g., C3—C4) are in the range of 0.1532–0.1583 nm.

The energies per one carbon atom of **16**–**20** relative to the graphene sheet are 96.65, 129.02, 136.97, 148.73, and 160.34 kJ mol^{-1}, respectively. This means that the prism carbon sheets are thermodynamically less stable than the graphene sheet. But these relative energies are not high enough to break bonds in the array, as considering the typical carbon–carbon bond energies (348, 614, and 839 kJ mol^{-1} for single-, double-, and triple bonds, respectively[29]).

The thickness of the prism carbon sheets is estimated to be about 0.49–0.50 nm from the longest vertical bond lengths (0.15–0.16 nm) and the standard van der Waals radius of carbon atom (0.17 nm). Therefore, this class of carbon allotropes can belong to the carbon nano-sheet family. The energies and bond lengths of **16**–**20** are listed in Table 1.

Exploration of prism carbon tube

Further exploration was made for carbon tube structures by axially connecting the C_n (n = 3–20) ring units of regular polygons.[21] The tube structures were optimized with using PBC of G09. To reduce computational demands and to remove difficulties of PBC calculations arising from large basis functions, PBC optimized structures of the prism carbon sheets were obtained at the RHF/STO-3G level. We chose this minimal-basis for ab initio calculations based on the studies on prism-C_{2n} and prism carbon sheets. We have been working on further investigations of periodic systems at higher levels. However, we describe here only the previous results,[20–22] that showed the main characteristics of periodic carbon systems enough at the level.

The initial unit cell contained a regular polygon structure C_n ring with an initial bond length of 0.150 nm. The initial one-dimensional translation vector was set to be at an angle of 90° with a spacing of 0.160 nm between the C_n ring units. In the PBC calculations, all coordinates were optimized through repeated procedures. The relative energies with respect to the monolayer graphene sheet were estimated at the same calculation level and were normalized per one carbon atom to compare between different sizes of carbon unit-cell.

Figure 12 shows the shapes of the explored prism-C_n tubes (n = 3–8, 10, 12, 14, 16, 18, and 20). All C_n rings were optimized to respective regular polygons, though the sizes were slightly changed from the initial ones; the bond lengths on the polygons (0.1526–0.1597 nm) were nearly equal to or only slightly longer than the typical CC single bond length of 0.154 nm. The optimized bond lengths between the neighboring polygons corresponding to the optimized translational vector along the tube axis are 0.1591–0.1614 nm, which are also only slightly longer than the single CC bond length of 0.154 nm. All carbon atoms are equivalent and connected with four neighboring carbon atoms via single bonds. This situation of four single-bond connections is similar to the sp^3 hybridization in diamond, but the large deformation from the tetrahedral angle may cause the elongation of the bonds slightly from the typical single bond.

The relative energies of the prism–C_n tubes per one carbon atom with respect to the energy value for graphene at the same level of electronic calculations were listed in Table 1 in comparison with other types of prism carbons. The most energetically stable one is the prism-C_5 tube. The second is the

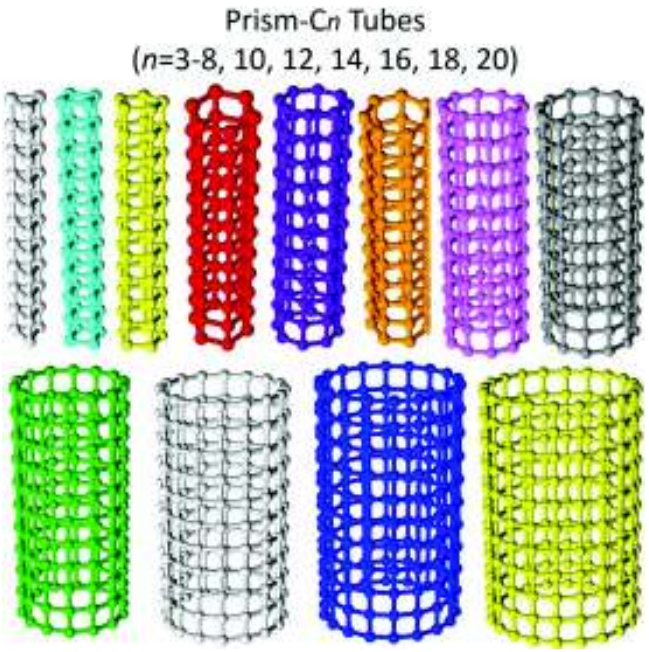

Figure 12. Prism-C_n tubes (n = 3–8, 10, 12, 14, 16, 18, and 20).

prism-C_6 tube, which is only slightly (9.1 kJ mol^{-1}) higher than the prism-C_5 tube. Appearance of the minimum in the relative energies may well be ascribed to the interplay between the decreasing steric strains in the polygons and the increasing steric strains of four neighboring bonds approaching the crossed connections at each carbon atom within a plane. We could not obtain larger prism tubes for n > 20, which seems to be due to the very strong strain in the nearly planar crossed geometry of four bonds at each carbon atom.

The radius of the polygon increases from 0.088 nm (n = 3) to 0.510 nm (n = 20). Accordingly, the outer size of each tube can be estimated as 0.258–0.680 nm by simply adding the van der Waals radius (0.17 nm) of a carbon atom. Prism tubes for n > 6 with radii larger than 0.17 nm can have an inner hole radius, which would be estimated as 0.01–0.34 nm by subtracting 0.17 nm from the radius of the respective polygon. Although the inner radii for n < 12 are too small to incorporate some molecules, large prism tubes of n = 12, 14, 16, 18, and 20 may possibly include small molecules such as H_2 in the inner holes.

Barrier heights around prism tube structures

To estimate the thermal stability of the prism tube structures, the barrier heights along reaction pathways surrounding the equilibrium geometries were studied for tri[4]prismane ($C_{12}H_8$) **21** and tri[6]prismane ($C_{18}H_{12}$) **22** by the SHS-ADDF method. ZPVE corrections were made for both of the equilibrium and transition structures. For reducing computation time, the large ADDF (LADD) and the FirstOnly options in GRRM14 were used. The LADD option limits ADDF to larger anharmonic downward distortions that cut off high energy pathways. The FirstOnly option limits the ADDF search only around the started equilibrium structure.

A $C_{12}H_8$ structure in a D_{4h} symmetry with a prism C_4-like carbon skeleton is known as dicubane (tri[4]prismane) **21**.[30–32] Starting from the structure of **21**, many reaction pathways were automatically explored at the B3LYP/6–31G(d) level. Figure 13A shows the lowest energy barrier pathway from the D_{4h} dicubane structure (EQ1) to the more stable D_{2h} dicubene[31] structure (EQ2) via the transition structure (TS1/2). The barrier height between EQ1 and TS1/2 was determined to be 81.6 kJ mol^{-1} after ZPVE corrections. In dicubene (EQ2), two CC bonds of the middle four-membered ring of dicubane (EQ1) are broken to produce a hexagonal prism structure with six four-membered rings on its side faces. In dicubene, four carbon atoms with no CH bonds constitute two sets of CC double bonds in a D_{2h} geometry. The dicubene structure was reported in the earlier study of **21**.[32] The structural change from dicubane to dicubene releases a large amount of isomerization energy of 473.0 kJ mol^{-1} after ZPVE corrections.

A $C_{18}H_{12}$ structure in a D_{6h} symmetry with a prism C_6-like carbon skeleton is known as tri[6]prismane **22**.[30] Starting from the structure of **22**, reaction pathways were automatically explored at the B3LYP/6–31G(d) level. Figure 13B shows the lowest energy barrier pathway from the D_{6h} structure of **22** (EQ1) to the more stable D_{3h} structure (EQ2) via the transition structure (TS1/2). The barrier height between EQ1 and TS1/2 was determined to be 83.6 kJ mol^{-1} after ZPVE corrections. In the D_{3h} structure (EQ2), six carbon atoms with no CH bonds constitute three sets of CC double bonds. The structural change from the D_{6h} structure to the more stable D_{3h} structure releases a large amount of isomerization energy of 475.8 kJ mol^{-1} after ZPVE corrections.

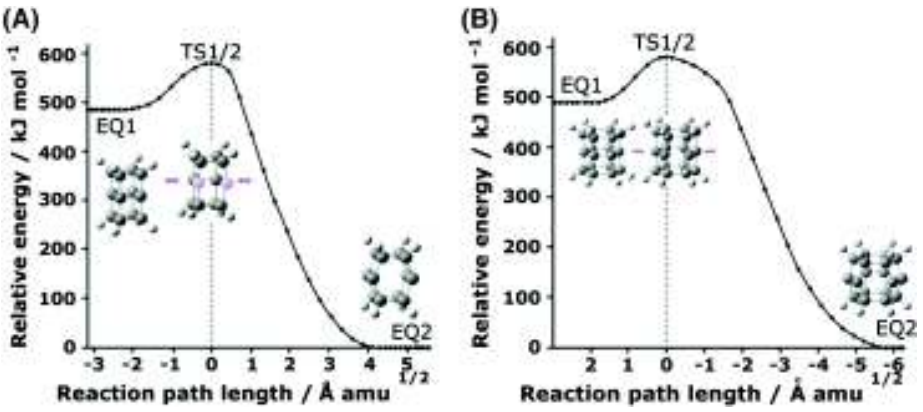

Figure 13. The lowest energy barrier pathways for **21** and **22**. A) The lowest pathway from the D_{4h} tri[4]prismane (**21**) structure of dicubane (EQ1) to the more stable D_{2h} structure of dicubene (EQ2) via the transition structure (TS1/2). B) The lowest pathway from the D_{6h} tri[6]prismane (**22**) structure (EQ1) to the more stable D_{3h} structure (EQ2) via the transition structure (TS1/2). Energies are shown without ZPVE corrections with respect to the lower energy equilibrium structure of EQ2. Reaction path lengths along the intrinsic reaction coordinates are shown with respect to the TS position in the standard unit of Å amu$^{1/2}$.

The values of about 80 kJ mol^{-1} obtained for the lowest energy barriers for D_{4h} $C_{12}H_8$ **21** and D_{6h} $C_{18}H_{12}$ **22** structures suggest that the prism-C_n tube structures can be thermally stable enough to exist. Note that the bond breaking only occurs at polygons and that the bond breaking does not occur at axial bonds along the tube axes. The lowest heights of barrier of prsim-C_{2n} and of prism carbon sheets were found to be about 150 kJ mol^{-1} and about 30 kJ mol^{-1}, respectively. It follows that the prism tubes are expected to be thermally more stable than the prism sheets. The relative ordering of the heights of the lowest barriers for the prism-C_{2n}, prism carbon sheets, and prism carbon tubes can be understood as follows. Tetravalent carbons in the prism sheets and tubes have the larger strains than formally trivalent carbons in the prism-C_{2n}, and thus the prism-C_{2n} are thermally more stable. Comparing the prism sheets with the prism tubes, the vertical bonds connecting polygons in the prism sheets are more easily broken. This is because the vertical bonds more easily stretch outside, whereas the stretching motions of the vertical bonds of the prism tube cause compression of the neighboring bonds along the straight lines on the side faces. The prism tube analogues of $C_{12}H_8$ and $C_{18}H_{12}$ exhibit bond breakings in the polygons, whereas the vertical bonds favor breaking in the prism-C_{2n} and the prism sheets.

Exploration of wavy carbons

The explorations of the wavy structures were initiated for $C_{2n}H_4$. Starting from flat ladder forms of $C_{2n}H_4$ (n = 3–20) with an initial distance of all CC bonds to be 0.14 nm, geometry optimizations were done. The explorations of wavy-C_{2n} (n > 10) were then conducted.[22] The geometry optimization calculations were started from regular polygon prism structures. The initial lengths of the bond in the polygon and the vertical bond were 0.144 and 0.150 nm, respectively. These calculations were done at the B3LYP/6–31G(d) level by using GRRM14.

Periodic wavy carbon structures were optimized by using PBC of G09. To reduce computational demands and to avoid the difficulties of PBC calculations arising from large basis functions, PBC optimizations were carried out at the RHF/STO-3G level. We chose this level for the minimal-basis ab initio calculations, because this series of structures is expected to follow the same tendency as that of prism-C_{2n} and prism carbon sheets, which do not show any substantial effect on the optimized bond connections by the different levels between RHF/STO-3G, RHF/3-21G, B3LYP/6–31G(d), B3LYP/6–311++(2d,2p), B3LYP/cc-pVDZ, and B3LYP/cc-pVTZ.

The initial structures of the periodic wavy structures were determined based on the results of $C_{2n}H_4$ and wavy-C_{2n} and of prism carbons. Wavy-C_n sheets (n = 2, 6, and 8) were produced by 2D-PBC energy-minimization calculations. One translational vector (Tv1) is along the wave direction of carbon chains including the C_n unit, and the other translational vector (Tv2) is along the straight arrays of edges of the rectangular four-membered rings. The initial length of Tv2 was set to be 0.160 nm, which was referred to a typical CC distance between the adjacent polygons in prism-C_n tubes. The initial lengths of Tv1 were set to be longer by increasing the number of atoms employed in the wave unit. The wavy-C_2 sheet means that a sheet with a unit cell consisting of two carbon atoms. In this case, carbon atoms along the wave direction are arranged to be an up–down form. The initial geometries of the wavy-C_2 sheet were determined by a manner as follows: The distance of the neighboring carbon atoms was set to be 0.160 nm, and the angle of three adjacent carbon atoms was set to be $\pm 120^\circ$ with the opposite sign between the neighbors as (–)(+) and so on. Thus, the initial length of the Tv1 was set to be $0.160 \times 3^{1/2} = 0.27713$ nm. The initial geometries of the wavy-C_6 sheet, consisting of six atoms in the unit cell, were determined by a manner as follows: The distance of the neighboring carbon atoms was set to be 0.160 nm, and the angle of three adjacent carbon atoms was set to be 120° with the ordering of signs to be (–)(–)(–)(+)(+)(+). The initial length of the Tv1 for the wavy-C_6 sheet was set to be $0.160 \times 3^{1/2} \times 2 = 0.55426$ nm. The initial geometries of the wavy-C_8 sheet, including eight atoms in the unit cell, were determined in a manner as follows: The distance of the neighboring carbon atoms was set to be 0.160 nm, and the angle of three adjacent carbon atoms was set to be 135° with the ordering of signs to be (–)(–)(–)(–)(+)(+)(+)(+). The initial length of the Tv1 for the wavy-C_8 sheet was set to be $0.160 \times (2^{1/2} + 1) \times 2 = 0.77255$ nm.

A wavy-C_{36} tube was produced by 1D-PBC energy-minimization calculations based on the wavy-C_{36}. The initial translational vector along the tube axis was set to be 0.160 nm.

The geometry optimizations starting from the flat ladder forms of $C_{2n}H_4$ (n = 3–20) gave various ladder-type structures. When the size was up to n = 8 ($C_{16}H_4$), we found that the ladder adopted a wavy form **23** (Fig. 14A). This C_{2h} structure of $C_{16}H_4$ clearly shows an interesting nature of a carbon ladder that preferentially adopts a wavy form in larger systems. Thus, we have investigated the structures by increasing the size up to n = 20, until obtaining a remarkably waving $C_{40}H_4$ **24** (Fig. 14B). After the geometry optimization calculations starting from regular polygon prism structures of C_{2n} (n > 10), they preferentially adopt wavy forms with concave polygons in various shapes **25**–**27** (Figs. 14C–14E) rather than forming convex polygons. We confirmed that the optimized geometries of **23**–**27** are definitely at the potential minima by the normal mode analyses showing no imaginary frequencies.

Stabilization energies through the geometry optimizations were in the range of 175–550 kJ mol^{-1}: **23**: 248.68, **24**: 550.01, **25**: 175.04, **26**: 205.14, and **27**: 235.85 kJ mol^{-1}. Any of the flat ladder forms of $C_{2n}H_4$ (n = 3–20) was stabilized to a convexly curved or a wavy form, and longer ladders showed larger stabilization energies. Any of the initial regular convex polygon prism structures of C_{2n} (n > 10) was stabilized also to wavy forms with concave polygons. The prism structures with larger polygons showed slightly larger stabilization energies. The height of the lowest barrier from **23** estimated with the SHS-ADDF method was 23.1 kJ mol^{-1}. This is a pathway to a convexly curved ladder form at 37.5 kJ mol^{-1} lower than **23**.

The four-membered rings appeared in **23**–**27** form nearly rectangular shapes. The bond angles along the long side (i.e., not at the rungs) of the ladder structures are mostly in the

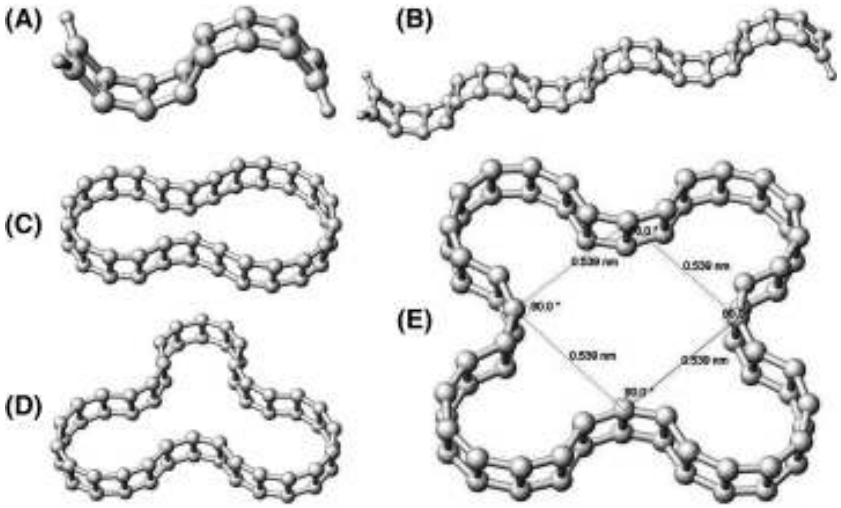

Figure 14. Various wavy forms of $C_{2n}H_4$ and C_{2n} optimized at the B3LYP/6–31G(d) level. A) $C_{16}H_4$(**23**), B) $C_{40}H_4$(**24**), C) C_{48}(**25**), D) C_{60}(**26**), and E) C_{72}(**27**).

range from 135° to 150°, which correspond to the inner angles of regular polygons from octagon to dodecagon. This finding is nearly correlated with the stability of the prism-C_{2n} (n = 8–10, 12) in Table 1. The CC bond lengths in the wavy ladders **23** and **24** are widely distributed in the range of 0.135–0.154 nm both for the longer sides and the rungs, whereas in the wavy form of the ring-closed ladders C_{2n} (**25**–**27**) the bond lengths in the polygons are 0.139–0.148 nm. They are mostly shorter than those of the side faces (0.147–0.159 nm). This distribution of the bond lengths is similar to that of the prism-C_{2n}: for example, in the prism-C_{20}, the lengths of the bond in the decagon and the vertical bond of prism-C_{20} (**12**) are 0.144 and 0.148 nm, respectively.

The wavy ring-closed ladders C_{2n} **25**–**27** form concave polygons that cause several dent parts, which increase with the number of atoms: two, three, and four dents appear in **25**, **26**, and **27**, respectively. This tendency seems to be related with the bond angle distributions between 135° and 150° in the opened ladder forms mentioned above, which can determine the limitation of the curvature of the ring-closed ladders.

The bond lengths are mostly shorter than the typical single CC bond length of 0.154 nm. This suggests their unsaturated characteristics, which can make additional bonds. This means that the wavy open- and closed-ladders are expected to become a unit of a sheet- or tube-type structures by connecting with each other at the both ends of the rungs.

The 2D-PBC calculations searching for the local minima gave three types of wavy carbon sheets **28**–**30** (Figs. 15A–15C), where lattices are cut at certain ranges, though the calculations were done for 2D-infinite systems. The PBC calculations were performed with the unit atoms and translational vectors specified in the respective figures in Figure 15.

The 1D-PBC calculation based on a wavy form of C_{72} in Figure 14E yielded wavy-C_{36} tube **31** (Fig. 16), where a range of 10 bonds along the tube axis are visualized, though calculations were done for the infinite system.

We estimated the energies per one carbon atom relative to graphene at the same level of the PBC calculations. The results are shown in Table 1 in comparison with other types of carbons. The relative energies of the wavy carbons **28**–**31** are comparable with the smaller prism-C_n tubes of n = 3, 6, and 8 but are much smaller than the larger prism-C_n tubes of n = 10, 12, 16, and 20. This indicates that the tetravalent carbon structures in the larger prism tubes hold strong steric strains, whereas the strains of the smaller prism tubes structures are not so severe. In the view of this tendency, the strains in the wavy carbons **28**–**31** are as moderate as the smaller prism tubes.

The bond lengths in the wavy carbons **28**–**31** are slightly longer than or even equal to the typical single bond length of 0.154 nm. This bond character is very similar to the prism tubes. The bonds along the straight-line directions (e.g., the C1 → C1′ direction in Figs. 15 and 16) of the wavy carbons **28**–**31** show nearly the same lengths of about 0.161 nm, which agree well with the corresponding bond lengths on the side face (between two polygons) of the prism-C_n tubes (n = 8–12). The bonds along the wavy (bend)-line direction in **28**–**31** are in the range of 0.153–0.160 nm, which is similar well to the bond lengths on the regular polygons of the prism tubes. The shortest bond lengths of 0.1528–0.1538 nm correspond with a typical single bond length of 0.154 nm.

For **28**–**31**, carbon-chains along the straight-line are exactly straight, that means, all of the bond angles along the line are 180°. The bond angles along the wavy-line are: 107.5° in **28**, 116.7° and 125.9° in **29**, 118.8° and 133.0° in **30**, 125.3°, 115.9°, 119.1°, 137.4°, and 147.0° in **31**. These angles correspond to the inner angles of polygons from pentagon (106°) to decagon (144°). This tendency may be related with the relative energies of **28**–**31**, which is also similar to the prism-C_n tubes (n = 5–10).

In **28**, all carbon sites are equivalent. Both sides of the sheet are also equivalent. All four-membered rings adopt the same rectangular shape. The directions of the straight carbon-chain axis and the up–down carbon-chain are mutually orthogonal on the sheet plane. The van der Waals thickness of **28** is estimated to be 0.431 nm by using van der Waals radius of carbon atoms 0.170 nm.

In **29**, there are only two types of carbon sites: *top* (C3 and C6 in Fig. 15B) and *edge* (C1, C2, C4, C5, and C7 in Fig. 15B). These two sites are assumed to show different chemical properties. Correspondingly, there are two types of rectangular

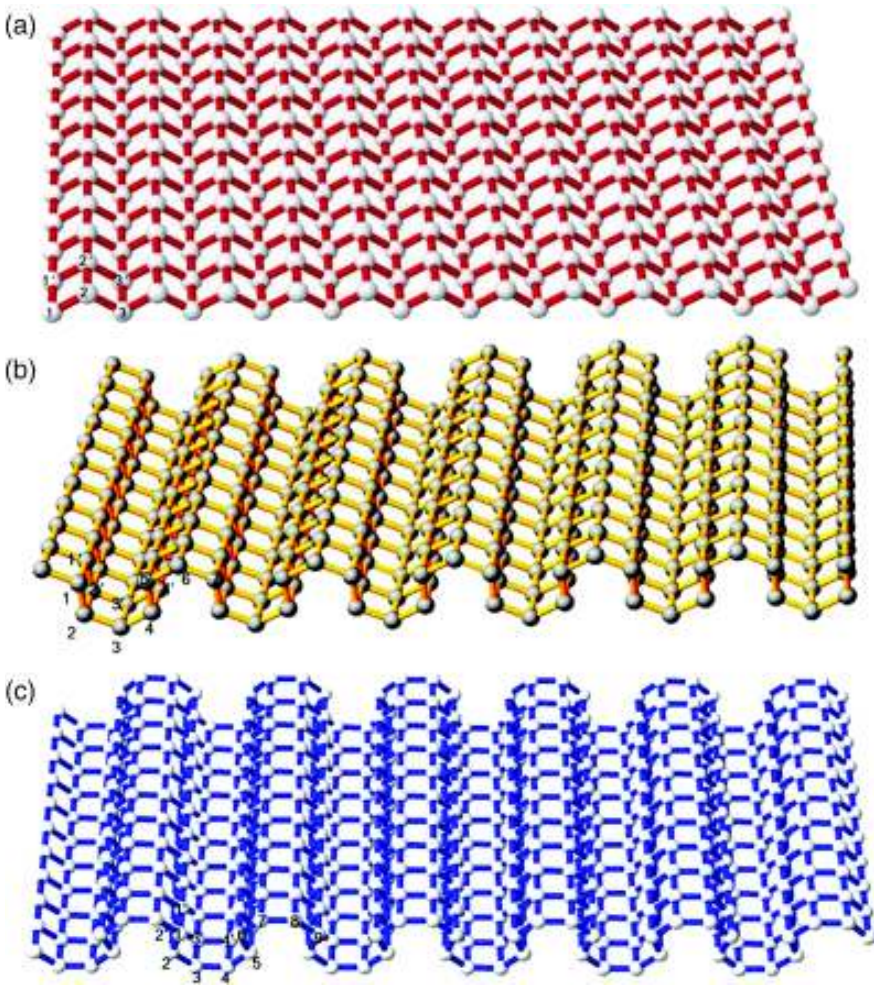

Figure 15. Wavy-C_n sheets. **A**) Wavy-C_2 sheet **28** obtained by 2D-PBC calculations with a unit of two atoms (1, 2). The translational vectors are 1–1′ (0.1608 nm) and 1–3 (0.2497 nm) with a mutual angle of 90°. CCC angle (1–2-3) is 107.52°. **B**) Wavy-C_6 sheet **29** obtained by 2D-PBC calculations with a unit of six atoms (1–6). The translational vectors are 1–1′ (0.1606 nm) and 1–7 (0.5604 nm) with a mutual angle of 90°. **C**) Wavy-C_8 sheet **30** obtained by 2D-PBC calculations with a unit of eight atoms (1–8). The translational vectors are 1–1′ (0.1607 nm) and 1–9 (0.6530 nm) with a mutual angle of 90°.

four-membered rings. Both sides of this sheet are equivalent. The van der Waals thickness of **29** is estimated to be 0.637 nm.

In **30**, there are only two types of carbon sites: *top* (C3, C4, C7, and C8 in Fig. 15C) and *edge* (C1, C2, C5, C6, and C9 in Fig. 15C). These two sites are assumed to show different chemical properties. There are three types of rectangular four-membered rings. Both sides of this sheet are equivalent. The van der Waals thickness of **30** is estimated to be 0.751 nm.

The shape of **31** shows a fourfold symmetry of D_{4h}. In **31**, there are five types of carbon sites, C1, C2, C3, C4, and C5 in Figure 16. Chemical properties of these sites are expected to be different. There are six types of rectangular four-membered rings. The outer van der Waals diameter of **31** is estimated to be 1.71 nm, and the diameter of the inner van der Waals hole is estimated to be about 0.2 nm. The size of the inner hole is large enough to contain some ions inside.

Regarding the geometrical stabilities, from the relative energies, bond lengths, and the bond angles, the present wavy carbon structures **28**–**31** are considered to be similar to the prism-C_n tubes of n = 5, 6, 7, and 8. The barrier height calculations for the infinite systems **28**–**31** are too difficult to carry out.

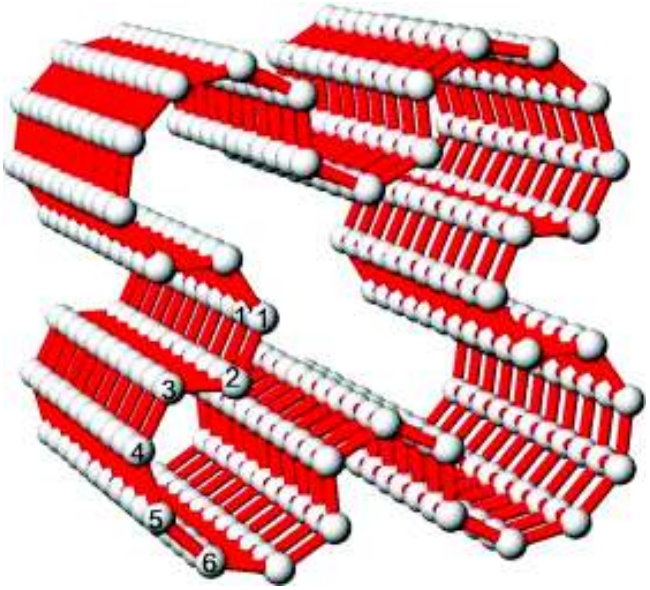

Figure 16. Wavy-C_{36} tube **31** obtained by 1D-PBC calculations with a unit of 36 atoms in a plane including 1–6. The translational vector is 1–1′ (0.1608 nm). All 36 atoms of the unit in a D_{4h} geometry are located on a plane perpendicular to the tube axis.

However, from the energy barriers about 80 kJ mol^{-1} obtained for tri[4]prismane ($C_{12}H_8$) **21** and tri[6]prismane ($C_{18}H_{12}$) **22** in the study on the similar system, prism-C_n tubes, we can infer that the wavy carbon structures **28**–**31** are also chemically and thermally stable enough at a similar level of the prism-C_n tubes.

We have to mention the long-range stability of periodic systems. There are some negative reports, which doubted the existence of 2D layers for 2D crystals[33,34] and large membranes.[35,36] These systems, however, are rather forced to be a flat plane structure, and most likely the constraint makes the systems unstable. In this respect, the wavy-carbon sheets **28**–**30** are different from those criticized systems. Our new sheets are not forced to hold the forms and are firmly constructed with tetravalent carbon atoms with four single bonds of ordinary bond lengths. Therefore, we consider that these wavy-sheets will show different characters from those other 2D layers and will be stable enough to exist.

Peculiar characteristics of carbon frames

During the search of new carbon allotropes given above, we found peculiar carbon atoms far from the tetravalent carbon atoms. EQ19 in Figure 1 as well as EQ171 and EQ298 in Figure 2 show 5–6 adjacent atoms around one carbon atom, which seem to be a hypervalent or hyper-coordinated carbon atom. These atypical hypervalent carbon atoms were studied on hexa-coordinated carbons of $(CH)_6^{2+}$[37–39] and also on the larger coordination numbers.[40,41] The SHS-ADDF method can explore not only typical but also atypical structures without any preconditions beforehand.

In contrast to the typical tetravalent carbon of sp^3 hybridization, the tetravalent carbons found in prism-C_n tubes, prism-C_{2n} sheets, and wavy carbons shown in Figures 9–12, 15, and 16 are far from the regular sp^3 tetrahedral structure. In the case of prism-C_{2n} sheets, three atoms are located in a trigonal or nearly trigonal directions within a plane, and the remaining one atom is arranged on a vertical direction, as can be seen in Figures 9–12. In other cases of prism-tubes and wavy carbons, a couple of adjacent atoms are arranged on a straight line, but another couple of adjacent atoms are arranged via the central atom in a bent configuration, as can be seen in Figures 15 and 16. Among the configurations in Figures 15 and 16, the angle among the bent array of three atoms is the largest (162°) for prism-C_{20} tube and the smallest (60°) for prism-C_3 tube. In the largest tube of prism-C_{20}, the bond angle along the polygon edge is 162°, which is only 18° smaller with respect to the completely linear case of 180° yielding the exactly cross-shaped tetravalent carbon configuration.

The prism and wavy carbon structures are highly energetic systems. Table 1 shows relative energies per one carbon atom for these carbon systems (denoted as energetic index EI). For the wavy, prism tube, and prism sheet carbon structures, the relative energies were measured with respect to graphene, at the RHF/STO-3G level. For the prsim-C_{2n}, the relative energies were measured with respect to fullerene C_{60}, at the B3LYP/6–31G(d) level. The highly energetic property of these structures may be ascribed to the highly strained local structures around carbon atoms. The prism and wavy carbon structures hold atypical steric configurations around carbon atoms, which are far from typical sp^3, sp^2, or sp hybridizations.

The prism-C_{2n} (n = 8–20) structures are slightly energetic with EI of about 130–140 kJ mol^{-1}. This level of EI is nearly two times as large as the EI for tetrahedrane **5**, which is estimated as 63.75 kJ mol^{-1}. EI for **5** can be estimated as 255/4 = 63.75 kJ mol^{-1}, since **5** has four carbon atoms and an extra chemical energy of 255 kJ mol^{-1} with respect to the global minimum isomer of vinylacetylene **1**.

The prism sheets are also slightly energetic with EI of about 100–160 kJ mol^{-1}. This is comparable to the most unstable isomer of C_4H_4 (EQ31 in Fig. 1) whose EI is estimated as 576.6/4 = 144.15 kJ mol^{-1}. This difference between the prism-C_{2n} and the prism sheets may be ascribed to their chemical bonding. As can be seen from the listed bond lengths in Table 1, the prism-C_{2n} structures have conjugated bond characters, whereas the prism sheets contain many bonds longer than or comparable to the typical single bond.

The prism tubes and wavy carbon structures are more highly energetic with EI of about 200–350 kJ mol^{-1}. This is because most bonds are clearly longer than the typical single bond. The bonds in prism tubes and wavy carbon structures are considered to be weak single bonds.

These energetic carbon allotropes may become ideal energy reservoirs, because energy can be charged or discharged with no consumption of additional materials nor production of waste materials. Transformation among various forms of carbons may be possible without additional materials. The first problem of the carbon allotropes is how to synthesize them. And the second problem is how to use them, that means, how to charge and discharge energy using the materials.

Preceding studies on carbon structures with four-membered rings

We have reviewed the carbon structures including four-membered rings as a key unit, which were recently found by our studies. However, some studies on carbon structures with four-membered rings were reported[42–54] prior to our studies. Last but not least, we wish to review the details of these preceding studies as comparing with our investigations.

A computational study on the isomers of C_4H_4 was reported in 2006.[42] They explored the PES by density functional theory (DFT), G2M, and CCSD(T), and found 31 EQs, 54 TSs, 11 DCs, and 8 minima that were rearranged to more stable structures by changing the calculation levels. The number of EQs is almost the same as that obtained from our exploration (32 EQs), whereas the number of TSs much smaller than that our results (171 TSs, see the first section of Results and Discussions). The difference is in the structures in high energy, such as carbenes and biradical structures. Further detailed computational studies will be needed to discuss these TS structures. An experimental and computational study on C_6H_4 in the context of the formation of *o*-benzyne was reported in 2011.[43] They investigated the detailed reaction pathways around *o*-benzyne.

The hydrocarbons in a ladder form were computationally investigated in 2001[44] and 2009,[45] and the curve shape of the ladder

hydrocarbons were reported as we saw in $C_{10}H_4$. The structures and energies of butalene and its homologues $C_{2n}H_4$ (n = 3–5) were studied in connection with aromaticity by DFT calculations at the BLYP/6–31G(d) level, and the curved ladder structures were observed from $n \geq 4$.[44] Extensive computational studies on cyclobutalenoids $C_{2n}H_4$ (n = 2–10) with B3LYP, CASSCF, and CCSD(T) methods resulted in curved ladder structures from $n \geq 3$.[45]

The first computational studies of [n]-prismanes ($C_{2n}H_{2n}$), hydrocarbons in a prism form, were reported in 1988.[46] They investigated the structures of $C_{2n}H_{2n}$ (n = 3–12) at the RHF/STO-3G, 3-21G, and 6–31G(d) levels within constrained geometries in a D_{nh} symmetry. Computational studies of [n]-prismanes at a higher level B3LYP/6–311 + G(2df,p) was reported in 2006.[47] They confirmed that [n]-prismanes (n = 3–10) are stable in a D_{nh} symmetry with no imaginary vibrational eigenvalues and that [n]-prismanes (n > 10) do not hold the D_{nh} prismatic configurations in the equilibrium state, whereas prism-C_{2n} (n = 3–20) hold the prismatic configuration up to n = 20. This difference infers that a prism form can favor carbon allotropes (e.g., prism-C_{2n}) rather than hydrocarbons (e.g., [n]-prismanes).

We have demonstrated the possibility of several types of polymers of the prism-C_{2n} unit with unsaturated bonds in this article. We came up with the idea of the polymerization by following the fact that carbon allotropes with unsaturated bonds can undergo polymerization reactions, for example, fullerene-C_{60}-polymers.[48–50] Some of the prism-C_{2n}-polymers in a sheet form can be categorized according to the classification rule of carbon structures based on hybridization and the number of connected covalent bonds reported in 2013.[51] For instance, prism-C_{12}-sheet-A (**16**), prism-C_{24}-sheet-C (**18**), and prism-C_{24}-sheet-D (**19**) belong to L_6 of the group [$2D_c$,4], L_{4-8} of the group [$2D_c$,4], and L_{4-6-12} of the group [$2D_c$, 4], respectively. The prism-C_n tubes are polymers of C_n monocyclic rings, which is similar to poly[n]prismanes (n = 3–6).[30–32] The size of the C_n monocyclic rings is limited to n < =6 to form poly[n] prismanes,[30] whereas at least the ring size up to n = 20 is possible to form prism-C_n tubes. The maximum number of the rings to polymerize is six for poly[n]prismanes giving $C_{28}H_8$,[32] whereas longer prism-C_n tubes can converge, and we have not found the limitation number of the polymerization.

The buckled graphene is a popular carbon allotrope with a wavy shape, where the neighboring carbon atoms are alternately raised and lowered.[52–54] This means, the six-membered ring in the buckled graphene is not flat. The wavy-C_n **23**–**27** form a similar wavy shape, however, any of the four-membered rings is flat. This similarity and the difference in carbon position can influence the property and stability of the structures.

Conclusions

This article presented our recent findings on carbon allotropes with four-membered ring structures in the context of the global exploration of potential energy surfaces. The new carbon allotrope family includes prism-C_{2n}, polymerized prism-C_{2n}, prism-C_{2n} sheets, prism-C_n tubes, and wavy-C_n. The basic unit is a C_n monocyclic ring structure, and the units are connected to each other in various combinations to form the structures. A common characteristic is that they consist of four-membered rings as a key unit. A four-membered ring is a known structure unit, which can be found in several organic molecules, for example, cubane, but has not been well studied as a unit of carbon allotropes compared to larger membered-rings, such as five- and six-membered rings. We determined the structures and energies with several levels of DFT calculations, confirmed the bond property with the QTAIM method, examined the lowest energy barrier from the equilibrium structure with the SHS-ADDF method, and concluded that these carbon structures have high energy but are located in a well deep enough to exist. Some of the bond lengths observed in the structures do not belong to any of typical carbon–carbon bond lengths. This atypical bond property can be categorized to a new chemical bonding.

The benefit of the structure exploration on quantum mechanical potential energy surfaces is that one can directly discuss the possibility of the existence based on the electronic structure and energy. If TS structures and energies not only EQ are obtained, more detailed discussions on the possibility of the existence are possible. The prediction presented in this article is supported by EQ and TS structures and energies with several DFT calculations. Further investigations with more precise or dynamics calculations will give more detailed information on this carbon allotrope family.

We have demonstrated the variety of carbon allotropes with four-membered rings. But we do not think that we have completed the exploration of structures belonging to this family. There must be another possible direction to explore. This is a challenging topic, which we have been working on indeed.

We believe that the exploration of structures and reactions on potential energy surfaces will show us more interesting science, and we will never forget the encouragement by Prof. Morokuma with his passion for chemistry.

Acknowledgment

The authors are very thankful to Professor Waro Nakanishi and Dr. Satoko Hayashi for the technical advice to use AIM 2000.

Funding information

Japan Society for the Promotion of Science (Challenging Exploratory Research), Grant/Award Number: 23655021 (to K.O.); Japan Society for the Promotion of Science (Challenging Exploratory Research), Grant/Award Number: 25540017 (to H.S.); Data Centric Science Research Commons Project of the Research Organization of Informatics and Systems (RIOS), Japan (to H.-S. and K.O.)

Keywords: potential energy surface exploration · carbon allotrope · four-membered ring carbon structure · high-energy material

How to cite this article: Koichi Ohno, H. Satoh, T. Iwamoto, H. Tokoyama, H. Yamakado. *J. Comput. Chem.* **2019**, 40, 14–28. DOI: 10.1002/jcc.25556

[1] R. B. Heimann, V. V. Ivanovskaya, Y. Koga, Carbon **1997**, 35, 1654.
[2] H. Kroto, J. E. Fisher, D. E. Cox, Eds., The Fullerenes, Pergamon Press, Oxford, **1993**.
[3] P. J. F. Harris, Carbon Nanotubes and Related Structures, Cambridge University Press, Cambridge, **1999**.
[4] A. K. Geim, K. S. Novoselov, Nat. Mater. **2007**, 6, 183.
[5] L. Pauling, The Nature of the Chemical Bond, 3rd ed., Cornell University Press, Ithaca, New York, **1960**.
[6] G. Povie, Y. Segawa, T. Nishihara, Y. Miyauchi, K. Itami, Science **2017**, 356, 172.
[7] F. Jensen, In Introduction to Computational Chemistry, 2nd ed.; Wiley: Chichester, West Sussex, England, **2007**; Ch. 12, pp. 380–420.
[8] H. B. Schlegel, J. Comput. Chem. **2003**, 24, 1514.
[9] K. Fukui, Acc. Chem. Res. **1981**, 14, 363.
[10] K. Ohno, S. Maeda, Chem. Phys. Lett. **2004**, 384, 277.
[11] S. Maeda, K. Ohno, J. Phys. Chem. A **2005**, 109, 574.
[12] K. Ohno, S. Maeda, J. Phys. Chem. A **2006**, 110, 8933.
[13] S. Maeda, K. Morokuma, J. Chem. Phys. **2010**, 132, 241102.
[14] S. Maeda, K. Morokuma, J. Chem. Theory Comput. **2011**, 7, 2335.
[15] S. Maeda, T. Taketsugu, K. Morokuma, J. Comput. Chem. **2014**, 35, 166.
[16] S. Maeda, K. Ohno, K. Morokuma, Phys. Chem. Chem. Phys. **2013**, 15, 3683.
[17] V. Georgakilas, J. A. Perman, J. Tucek, R. Zboril, Chem. Rev. **2015**, 115, 4744.
[18] M. Takagi, T. Taketsugu, H. Kino, Y. Tateyama, K. Terakura, S. Maeda, Phys. Rev. B **2017**, 95, 184110.
[19] K. Ohno, H. Satoh, T. Iwamoto, Chem. Lett. **2015**, 44, 712.
[20] K. Ohno, H. Satoh, T. Iwamoto, Chem. Phys. Lett. **2015**, 633, 120.
[21] K. Ohno, H. Tokoyama, H. Yamakado, Chem. Phys. Lett. **2015**, 635, 180.
[22] K. Ohno, H. Satoh, T. Iwamoto, H. Tokoyama, H. Yamakado, Chem. Phys. Lett. **2015**, 639, 178.
[23] M. J. Frisch, G. W. Trucks, H. B. Schlegel, G. E. Scuseria, M. A. Robb, J. R. Cheeseman, G. Scalmani, V. Barone, B. Mennucci, G. A. Petersson, H. Nakatsuji, M. Caricato, X. Li, H. P. Hratchian, A. F. Izmaylov, J. Bloino, G. Zheng, J. L. Sonnenberg, M. Hada, M. Ehara, K. Toyota, R. Fukuda, J. Hasegawa, M. Ishida, T. Nakajima, Y. Honda, O. Kitao, H. Nakai, T. Vreven, J. A. Montgomery, Jr., J. E. Peralta, F. Ogliaro, M. Bearpark, J. J. Heyd, E. Brothers, K. N. Kudin, V. N. Staroverov, R. Kobayashi, J. Normand, K. Raghavachari, A. Rendell, J. C. Burant, S. S. Iyengar, J. Tomasi, M. Cossi, N. Rega, J. M. Millam, M. Klene, J. E. Knox, J. B. Cross, V. Bakken, C. Adamo, J. Jaramillo, R. Gomperts, R. E. Stratmann, O. Yazyev, A. J. Austin, R. Cammi, C. Pomelli, J. W. Ochterski, R. L. Martin, K. Morokuma, V. G. Zakrzewski, G. A. Voth, P. Salvador, J. J. Dannenberg, S. Dapprich, A. D. Daniels, Ö. Farkas, J. B. Foresman, J. V. Ortiz, J. Cioslowski, D. J. Fox, Gaussian 09, Revision D.01, Gaussian, Inc, Wallingford, CT, **2009**.
[24] S. Maeda, Y. Harabuchi, Y. Osada, T. Taketsugu, K. Morokuma, K. Ohno, GRRM14; **2014**. Available at: http://iqce.jp/GRRM/index_e.shtml (accessed on April 28, **2018**).
[25] R. F. W. Bader, Atoms in Molecules: A Quantum Theory, Oxfor University Press, New York, **1990**.
[26] F. Biegler-König, J. Comput. Chem. **2000**, 21, 1040.
[27] S. Maeda, K. Ohno, Chem. Phys. Lett. **2008**, 460, 55.
[28] K. Ohno, S. Maeda, Phys. Scr. **2008**, 78, 058122.
[29] G. N. Lewis, J. Am. Chem. Soc. **1916**, 38, 762.
[30] R. M. Minyaev, V. J. Minkin, T. N. Gribanova, A. G. Starikov, R. Hoffmann, J. Org. Chem. **2003**, 68, 8588.
[31] E. T. Seidl, H. F. Shaefer, III., J. Am. Chem. Soc. **1991**, 113, 1915.
[32] F. L. Lieu, L. Peng, J. Mol. Struct. THEOCHEM **2004**, 710, 164.
[33] N. D. Mermin, H. Wagner, Phys. Rev. Lett. **1966**, 17, 1133.
[34] N. D. Mermin, Phys. Rev. **1968**, 176, 250.
[35] K. S. Novoselov, D. Jiang, F. Schedin, T. J. Booth, V. V. Khotkevich, S. V. Morozov, A. K. Geim, Proc. Natl. Acad. Sci. USA **2005**, 102, 10451.
[36] K. S. Novoselov, Science **2004**, 306, 666.
[37] H. Hogeveen, P. W. Kwant, Tetrahedron Lett. **1973**, 19, 1665.
[38] H. T. Jonkman, W. C. Nieuwpoort, Tetrahedron Lett. **1973**, 19, 1671.
[39] H. Hogeveen, P. W. Kwant, Acc. Chem. Res. **1975**, 8, 413.
[40] V. I. Minkin, R. M. Minyaev, Mendeleev Commun. **2004**, 14, 43.
[41] Y. Wang, Y. Huang, R. Liu, Chemistry **2006**, 12, 3610.
[42] D. Cremer, E. Kraka, H. Joo, J. A. Stearns, T. S. Zwier, Phys. Chem. Chem. Phys. **2006**, 8, 5304.
[43] F. Zhang, D. Parker, Y. S. Kim, R. I. Kaiser, A. M. Mebel, Astrophys. J. **2011**, 728, 141.
[44] P. M. Warner, G. B. Jones, J. Am. Chem. Soc. **2001**, 123, 10322.
[45] S. Sakai, T. Udagawa, Y. Kita, J. Phys. Chem. A **2009**, 111, 13964.
[46] R. L. Disch, J. M. Schulman, J. Am. Chem. Soc. **1988**, 110, 2102.
[47] T. N. Gribanova, R. M. Minyaev, V. I. Minkin, Doklady Chem. **2006**, 411, 193.
[48] Y. Iwasa, Y. Iwasa, T. Arima, R.M. Fleming, T. Siegrist, O. Zhou, R.C. Haddon, L.J. Rothberg, K.B. Lyons, H.L. Carter, Jr., A.F. Hebart, R. Tycko, G. Dabbagh, J.J. Krajewski, G.A. Thomas, Y. Yagi Science **1995**, 264, 1570.
[49] X. Chen, S. Yamanaka, Chem. Phys. Lett. **2002**, 360, 501.
[50] S. Yamanaka, S. Yamanaka, A. Kubo, K. Imura, K. Komaguchi, N.S. Kini, T. Inoue, T. Irifune Phys. Rev. Lett. **2006**, 96, 076620.
[51] E. A. Belenkov, V. A. Greshnyakov, Phys. Solid Stat. **2013**, 55, 1754.
[52] J. M. Carlsson, Nat. Mater. **2007**, 6, 801.
[53] M. A. Kahn, M. A. Mukaddam, U. Schwingenshlögl, Chem. Phys, Lett. **2010**, 498, 157.
[54] O. Zhu, A. R. Oganov, A. O. Lyakbov, CrystEngComm **2012**, 14, 3596.

Received: 30 May 2018
Revised: 13 July 2018
Accepted: 24 July 2018
Published online on 3 October 2018